MARTIN MARIETTA ENERGY SYSTEMS LIBRARIES
3 4456 0150239 3

NUREG/CR-0501
(ORNL/NUREG/TM-279)

cy. 29

Advanced Two-Phase Instrumentation Program Quarterly Progress Report for April–June 1978

K. G. Turnage
P. A. Jallouk

Prepared for the U.S. Nuclear Regulatory Commission
Office of Nuclear Regulatory Research
Under Interagency Agreements DOE 40-551-75 and 40-552-75

ORNL TECHNICAL INFORMATION DIVISION
Y-12 TECHNICAL LIBRARY
Document Reference Section
LOAN COPY ONLY
Do NOT transfer this document to any other person. If you want others to see it, attach their names, return the document, and the Library will arrange the loan as requested.
UCN-1624
(3 5-60)

OAK RIDGE NATIONAL LABORATORY
OPERATED BY UNION CARBIDE CORPORATION · FOR THE DEPARTMENT OF ENERGY

Printed in the United States of America. Available from
National Technical Information Service
U.S. Department of Commerce
5285 Port Royal Road, Springfield, Virginia 22161

This report was prepared as an account of work sponsored by the United States Government. Neither the United States nor any of its employees, nor any of its contractors, subcontractors, or their employees, makes any warranty, express or implied, or assumes any legal liability or responsibility for the accuracy, completeness or usefulness of any information, apparatus, product or process disclosed, or represents that its use would not infringe privately owned rights.

NUREG/CR-0501
ORNL/NUREG/TM-279
Dist. Category R2

Contract No. W-7405-eng-26

Engineering Technology Division

ADVANCED TWO-PHASE INSTRUMENTATION PROGRAM QUARTERLY PROGRESS REPORT FOR APRIL—JUNE 1978

K. G. Turnage P. A. Jallouk

Manuscript Completed — December 20, 1978
Date Published — January 1979

NOTICE: This document contains information of a preliminary nature. It is subject to revision or correction and therefore does not represent a final report.

Prepared for the
U.S. Nuclear Regulatory Commission
Office of Nuclear Regulatory Research
Under Interagency Agreements DOE 40-551-75 and 40-552-75

NRC FIN No. B0401

Prepared by the
OAK RIDGE NATIONAL LABORATORY
Oak Ridge, Tennessee 37830
operated by
UNION CARBIDE CORPORATION
for the
DEPARTMENT OF ENERGY

MARTIN MARIETTA ENERGY SYSTEMS LIBRARIES
3 4456 0150239 3

CONTENTS

	Page
ABSTRACT	1
1. INTRODUCTION	1
2. EXPERIMENT DESCRIPTION	5
2.1 Loop Description	5
2.2 Instrumentation and Electronics	5
3. DATA REDUCTION METHOD	11
4. EXPERIMENTS PERFORMED	15
5. RESULTS	16
5.1 Individual Instrument Response	16
5.2 Mass Flux Calculations	28
6. SUMMARY AND CONCLUSIONS	36
REFERENCES	37

ADVANCED TWO-PHASE INSTRUMENTATION PROGRAM QUARTERLY PROGRESS REPORT FOR APRIL—JUNE 1978

K. G. Turnage P. A. Jallouk

ABSTRACT

Testing of advanced spool piece I is in progress. Two-phase air-water tests have been performed with several experimental drag targets. Results in this report are from one of the experiments performed with the spool piece oriented horizontally and with the drag flowmeter transducer fittings on top of the pipe. In an effort to better understand the capabilities of current spool piece instrumentation, several two-phase models have been used to analyze the data.

1. INTRODUCTION

The measurement of two-phase mass flow rate is of primary importance in experimental programs involving loss-of-coolant studies. Because of the severe environments present during blowdown, relatively few instrument types have gained widespread acceptance; these include turbine meters, gamma densitometers, and drag flowmeters. (Pressure and temperature measurements are also required for reduction of data from the other instruments.)

In the Thermal-Hydraulic Test Facility (THTF) at Oak Ridge National Laboratory (ORNL)[1] and in the semiscale facility at Idaho National Engineering Laboratory (INEL),[2] three full-flow instruments have been located in a relatively short piping segment called a spool piece. The design of spool pieces is important because the turbine meter and drag flowmeter are intrusive and may seriously alter the flow regime.[3] On the other hand, location of all three instruments in close proximity is desirable because of the often unsteady and inhomogeneous nature of two-phase flow.

The advanced spool piece[4] being used in the current studies is shown in Figs. 1.1 and 1.2. Its unique attributes include allowance for two drag body flowmeters and three flow-dispersing screens. The drag transducers used are like those in use for some time at ORNL, but several

ORNL–DWG 77–8598A

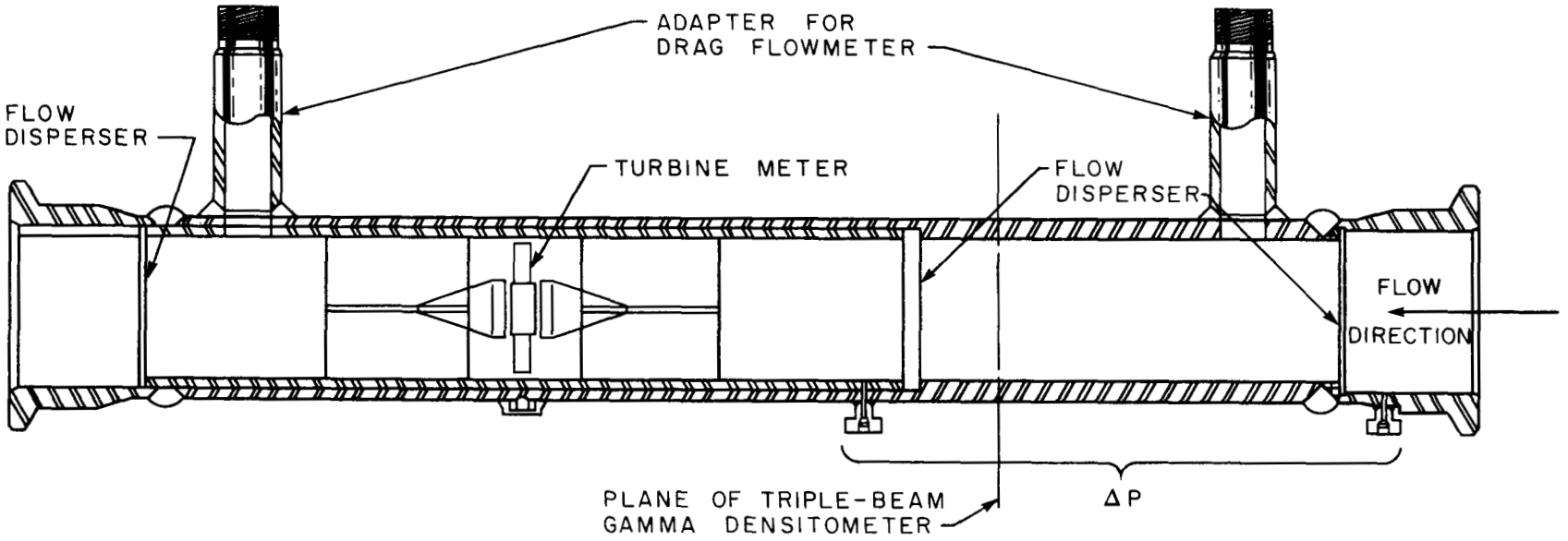

Fig. 1.1. Schematic diagram of advanced spool piece I.

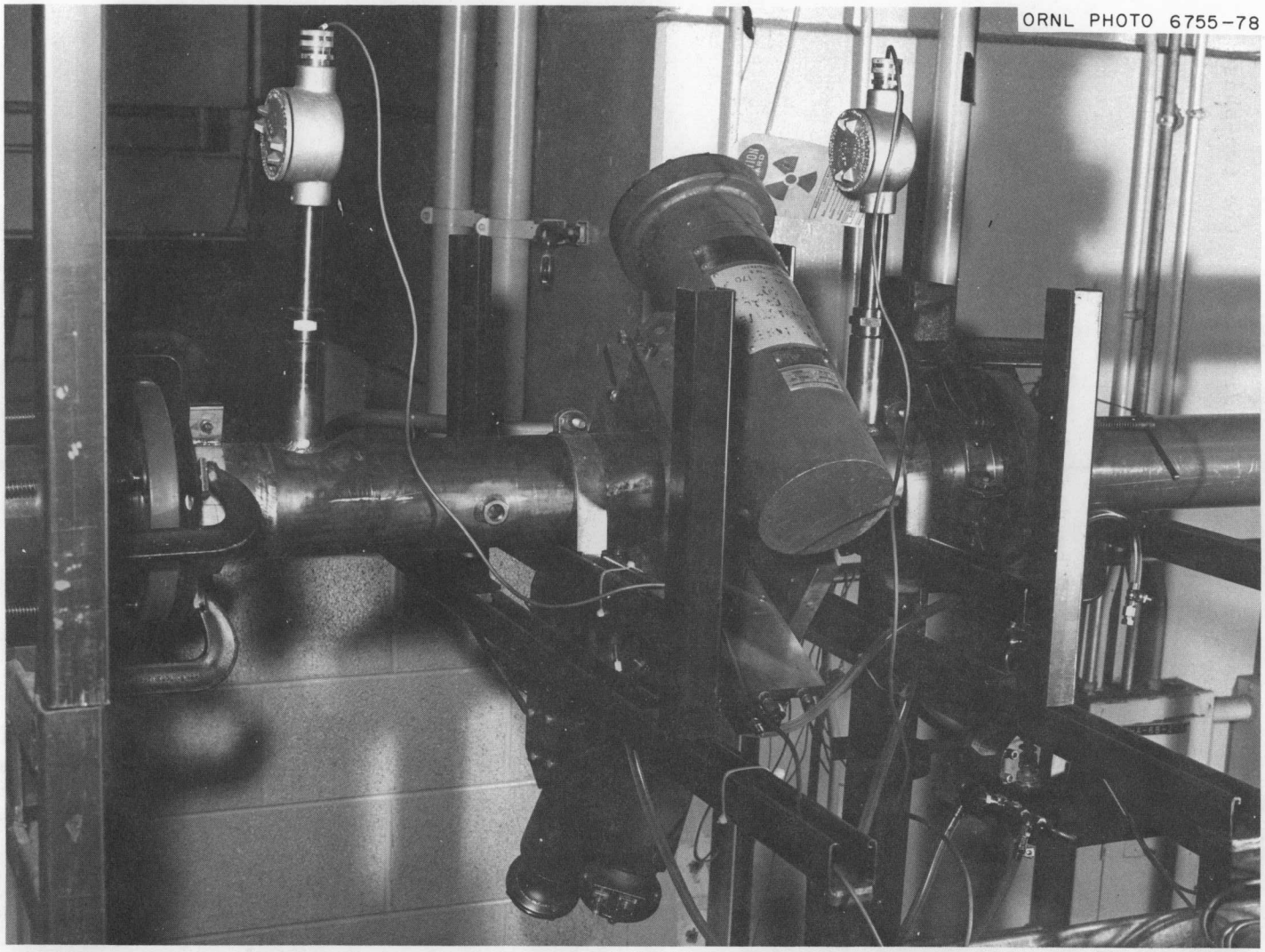

Fig. 1.2. Advanced spool piece I in ORNL air-water loop.

experimental drag targets have been tested. Also, a three-beam gamma densitometer and an 8.9-cm (3.5-in.) full-flow turbine meter are being used. When flow-dispersing screens are in the spool piece, pressure difference measurements may be used as an indication of the two-phase momentum flux.[5]

This report will describe the experimental facility used and the methods of data acquisition and reduction. Preliminary results from one of the experiments will also be described.

2. EXPERIMENT DESCRIPTION

2.1 Loop Description

The ORNL two-phase air-water loop (Fig. 2.1) is capable of supplying air at flow rates up to 242 liters/sec (512 scfm) and water at flow rates up to 32 liters/sec (500 gpm). In the 8.9-cm-ID (3.5-in.) spool piece tested, those rates correspond to superficial velocities of 39 m/sec (128 fps) for air and 5.2 m/sec (17 fps) for water. (When elements of large hydraulic resistance are in the loop, the highest two-phase flow rates are often not obtainable.) For this study, some 4.6 m (15 ft) of straight, clear 4-in. polyvinyl chloride (PVC) piping was located upstream of the stainless steel test section and some 1.2 m (4 ft) was located downstream. The single-phase air and water flows were at ambient temperature and near atmospheric pressure.

In the air-water loop, air flow rate is determined using a pressure gage upstream of the critical flow orifices, and water is metered into the loop by means of rotometers [flow rates 6.3 liters/sec (100 gpm)] or by a magnetic flowmeter. Air flow rates of 16, 32, 64, 128, 256, and 512 scfm with water flow rates of 10, 20, 30, 40, 60, 100, 150, 200, 250, 300, 350, 400, 450, and 500 gpm were used. No special measures were taken to enhance mixing, but the observed flow regimes in the horizontal section were in good agreement with the flow regime map of Mandhane et al.[6] (Fig. 2.2).

The experiment was conducted by setting the desired air flow rate and then taking data at successively higher water input rates until either the system pressure became high enough to unchoke the critical flow orifice or one of the instruments was overranged. The air flow rate was then doubled, and the procedure of taking data with various water flow rates was repeated.

2.2 Instrumentation and Electronics

A schematic of the electronics and the data acquisition system (DAS) used is shown in Fig. 2.3. In general, the signal output from each

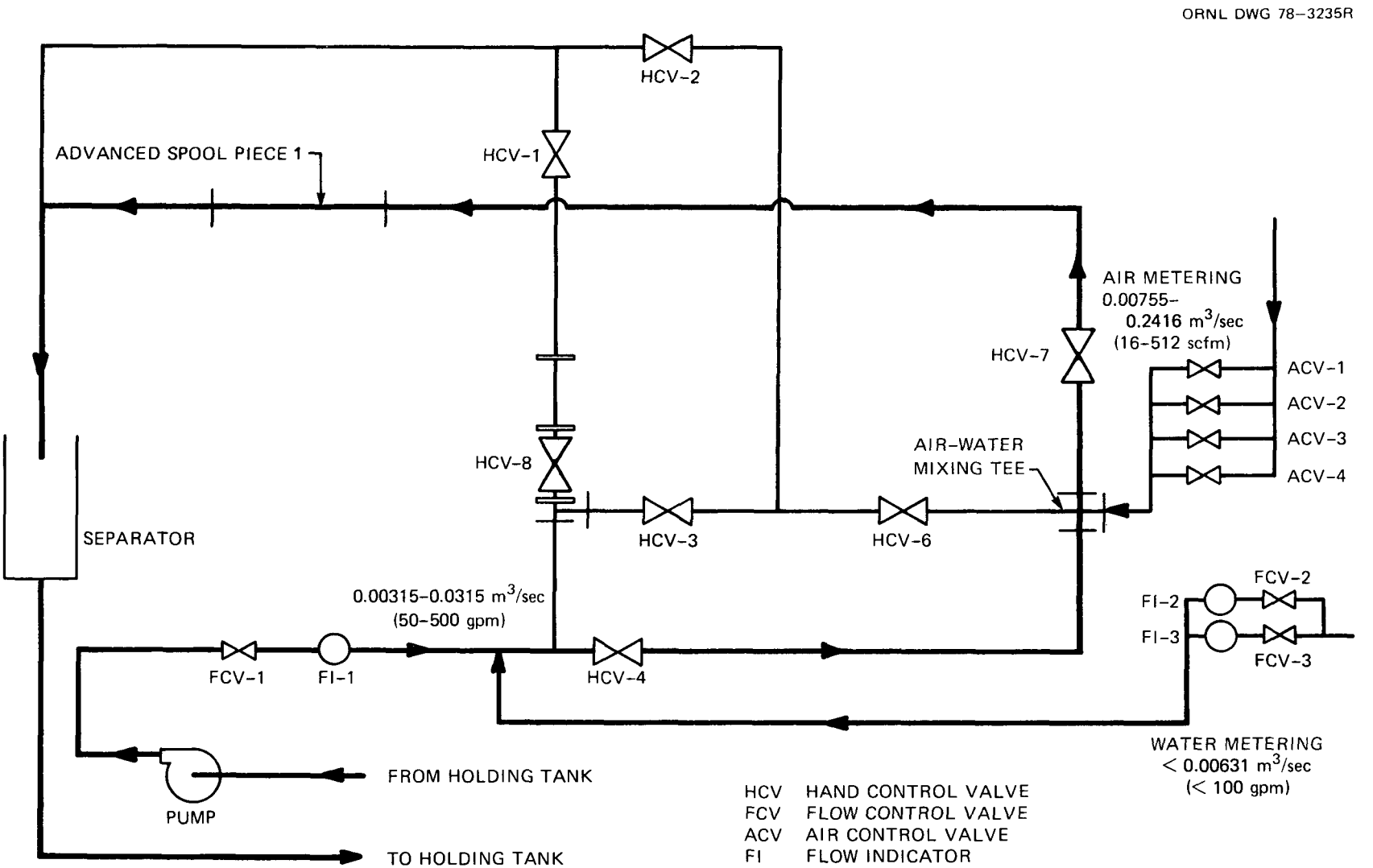

Fig. 2.1. Schematic diagram of ORNL air-water loop. Heavy line indicates flow path for current tests.

ORNL–DWG 78–20888

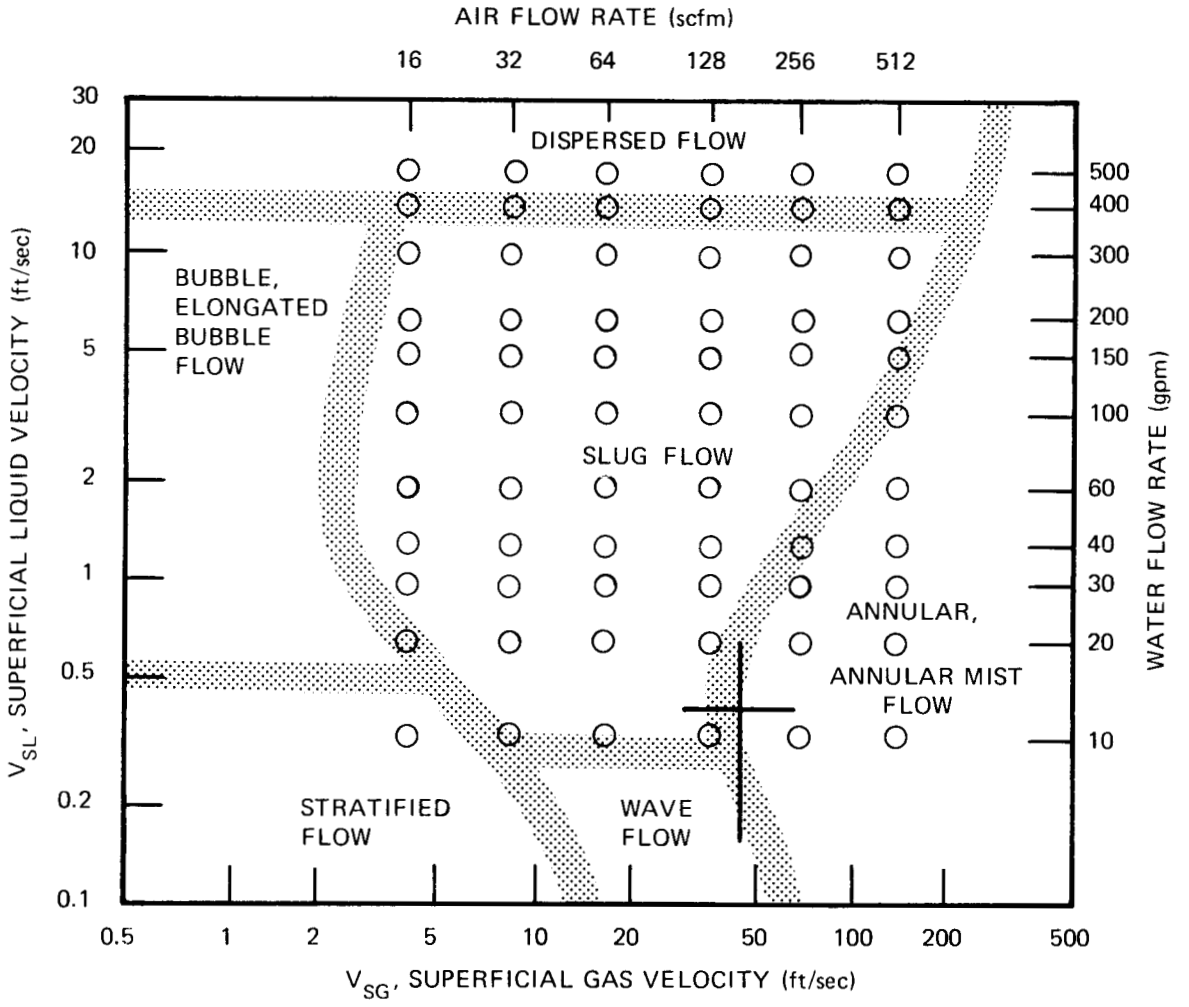

Fig. 2.2. Flow pattern map proposed by Mandhane et al.[6] with locations of data points used in current air-water studies.

instrument was processed by an appropriate set of electronics and then sent to the DAS (a PDP-8 computer and magnetic tape unit) and to an integrating digital voltmeter. The voltmeter was used to monitor the various instrument readings during the test. Instantaneous instrument readings from the computer were also printed for comparison with voltmeter readings during the test. During a data scan, data from the spool piece instrumentation were recorded on computer tape with a frequency of at least 500 values/sec.

The three-beam gamma attenuation densitometer was operated with controls and signal-conditioning equipment built by Measurements, Inc.

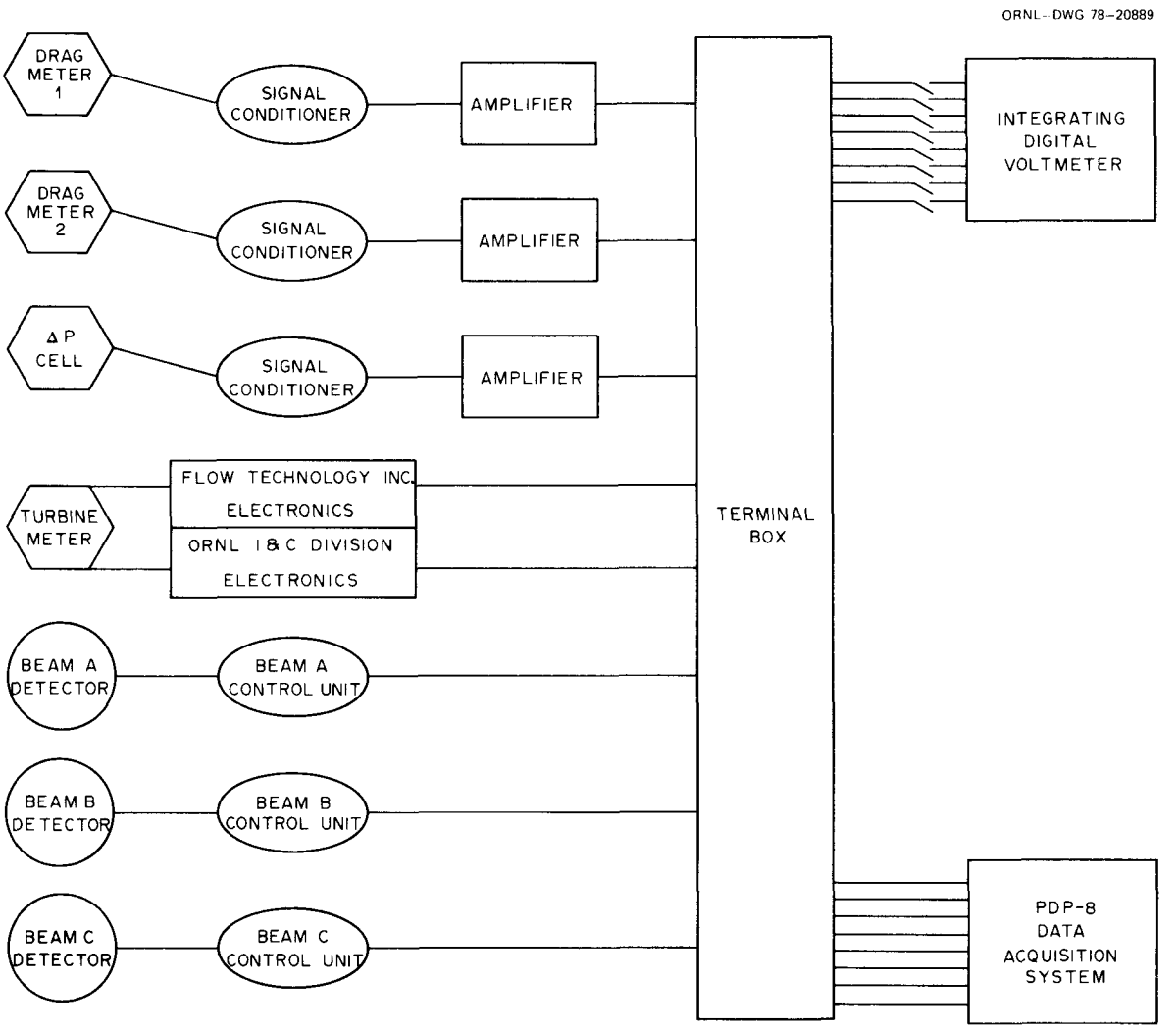

Fig. 2.3. Electronics and data acquisition system used for air-water studies.

The densitometer used sodium-iodide scintillation-crystal photomultiplier tube detectors that yielded a voltage output proportional to the counting rate. High voltages to the photomultiplier tubes were adjusted before the test so that the final output signal with the pipe empty was ∿9.5 V for each beam. (The maximum signal for input to the PDP-8 DAS is 10.0 V.) For purposes of calibration, the densitometer output voltages with the pipe full of water, empty, and with the ^{137}Cs gamma radiation source stored were recorded for each of the three beams. To allow for drift in the electronics, the calibration data were taken before and after the experiment.

The drag flowmeter transducers (Ramapo Instrument Company model Mark V-4PBRDX) consisted of strain gage type bridges with an excitation voltage of 5.0 V applied to each bridge using an Endevco model 4471.1A bridge conditioner. The differential output from the signal conditioners was then amplified by Princeton Applied Research Model 113 amplifiers, each of which was dc coupled. Frequency rolloff was not used.

Two sets of electronics were used with the Flow Technology Inc. turbine meter model FT-56I1000-L3 (see Fig. 2.4). One set was the Flow Technology model PRI-102AFR flow monitor supplied with the turbine; data to be presented in this report are from those electronics. The other set

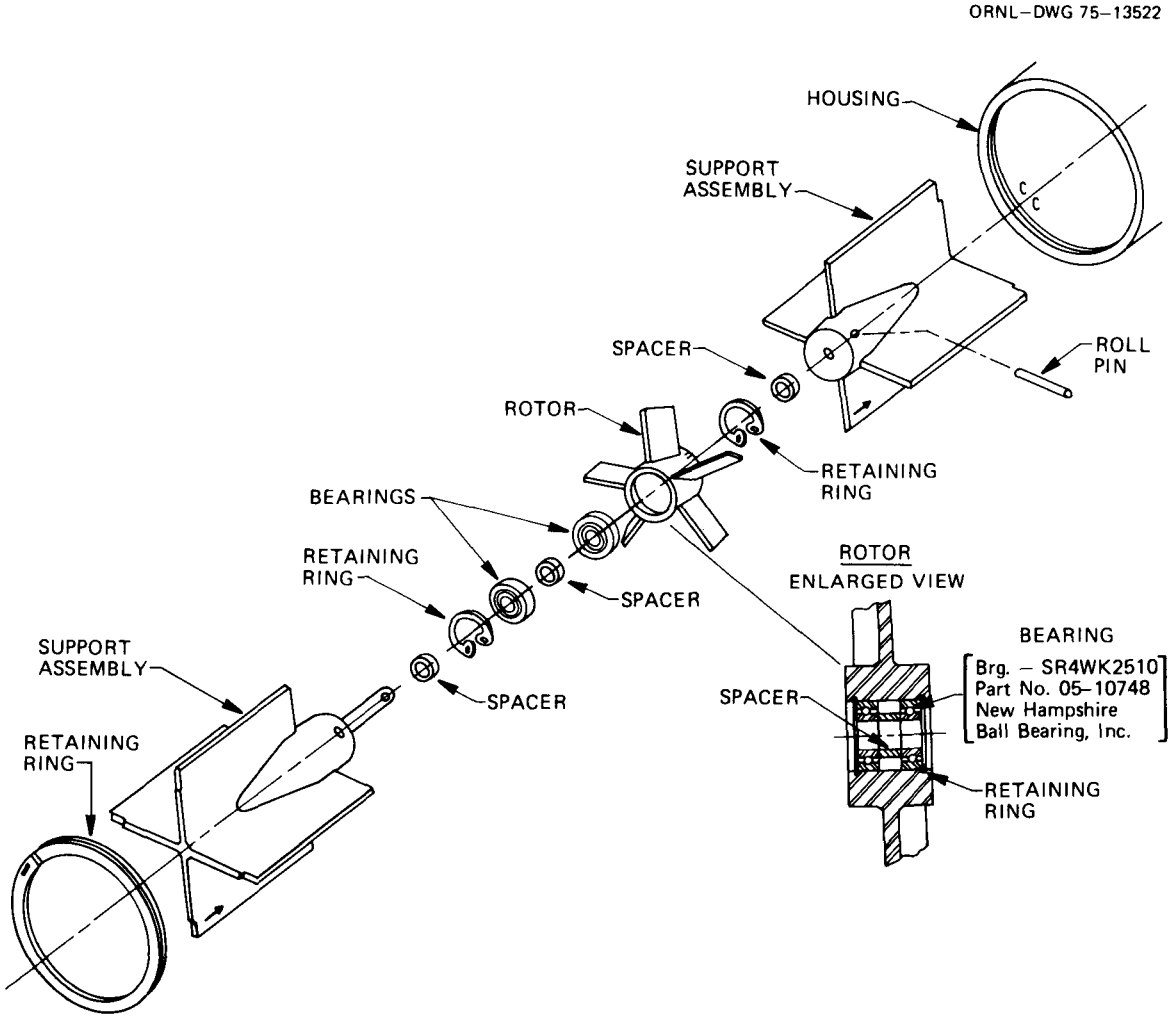

Fig. 2.4. Flow Technology Inc. turbine meter — exploded view.

was developed by the Instrumentation and Controls Division at ORNL. For the later runs, the output from both sets of electronics was recorded by the DAS.

3. DATA REDUCTION METHOD

The output tapes from the PDP-8 DAS are being analyzed using an IBM FORTRAN program.[7] Basically, the code performs an average of each reading over the period of a scan. The code then uses the measured values to calculate ∿50 quantities of interest (e.g., experimental parameters and flow rates predicted using two-phase models). Another FORTRAN program is then used to plot any two of the calculated variables vs each other.

In the code, an average density $\overline{\rho}$, velocity V_t, and fluid momentum flux I_d are calculated from the instrument output for use in two-phase models. Using the Flow Technology electronics, the turbine meter was calibrated against the magnetic flowmeter used to meter the higher water flow rates during the two-phase tests. A least-squares fit of the turbine output voltage data led to the calibration equation used:

$$V_t = 2.6247 \cdot V_{to} - 0.2181 \ , \tag{1}$$

where V_{to} is the voltage output of the turbine electronics in volts and V_t is the indicated velocity in feet per second.

The measured momentum flux depends on the particular drag target being tested. The calibration equation chosen was of the form

$$I_d = aV_{do}^b \ , \tag{2}$$

where V_{do} is the drag disk electronics output (V) and I_d is the indicated momentum flux ($lb_m/ft\text{-}sec^2$). With 5.0 V excitation applied and an amplification factor of 1000× used, the appropriate coefficients a and b used are as shown in Table 1 in the previous quarterly report.[8]

For initial studies with advanced spool piece I, a composite density in the pipe, $\overline{\rho}_r$, was calculated from the three average densities ρ_A, ρ_B, and ρ_C deduced from the individual beam signals. For a single, narrowly collimated photon beam (assuming the layers of material encountered by the beam are in series), the general expression for void fraction α is[9]

$$\alpha = \frac{\ln\ (I_{2\phi}/I_\ell)}{\ln\ (I_g/I_\ell)} \ , \tag{3}$$

where $I_{2\phi}$, I_g, and I_ℓ are the intensities of the detected gamma beams for two-phase fluid, the vapor only, and the liquid only, respectively. Also,

$$\rho = (1 - \alpha)\rho_f + \alpha\rho_g \ , \tag{4}$$

where ρ_f and ρ_g are the nominal densities of the liquid and vapor phases, respectively. In the case of air-water experiments, the second term may be neglected.

Substituting Eq. (3) into Eq. (4) and simplifying, we obtain

$$\rho = \rho_f \ \ln\ (I_\ell/I_g)\ \ln\ (I_g/I_{2\phi}) \ . \tag{5}$$

Each of the intensities I_i in Eq. (5) is assumed to be related to the difference of the densitometer voltage output at that condition and the voltage output with the source stored V_s. Thus,

$$\rho = \rho_f \ \ln \left(\frac{V_\ell - V_s}{V_g - V_s}\right) \ln \left(\frac{V_g - V_s}{V_{2\phi} - V_s}\right). \tag{6}$$

In practice, data reduction was performed using the equation

$$\rho = A \ \ln \ \frac{B}{V - V_s} \ , \tag{7}$$

where A, B, and V_s were updated for each data point, assuming a linear drift of the calibration voltages with time during the experiment, and V is the instantaneous output voltage of a detector. An average density ρ_i is calculated for each beam i at each time point during the scan. An average density for each beam over the time was then used for input to the three-beam gamma densitometer model.

A cross-section of the configuration of the steel spool piece and the three densitometer beam paths appears in Fig. 3.1. Three annular regions of homogeneous density are assumed. The average density ρ_i indicated by

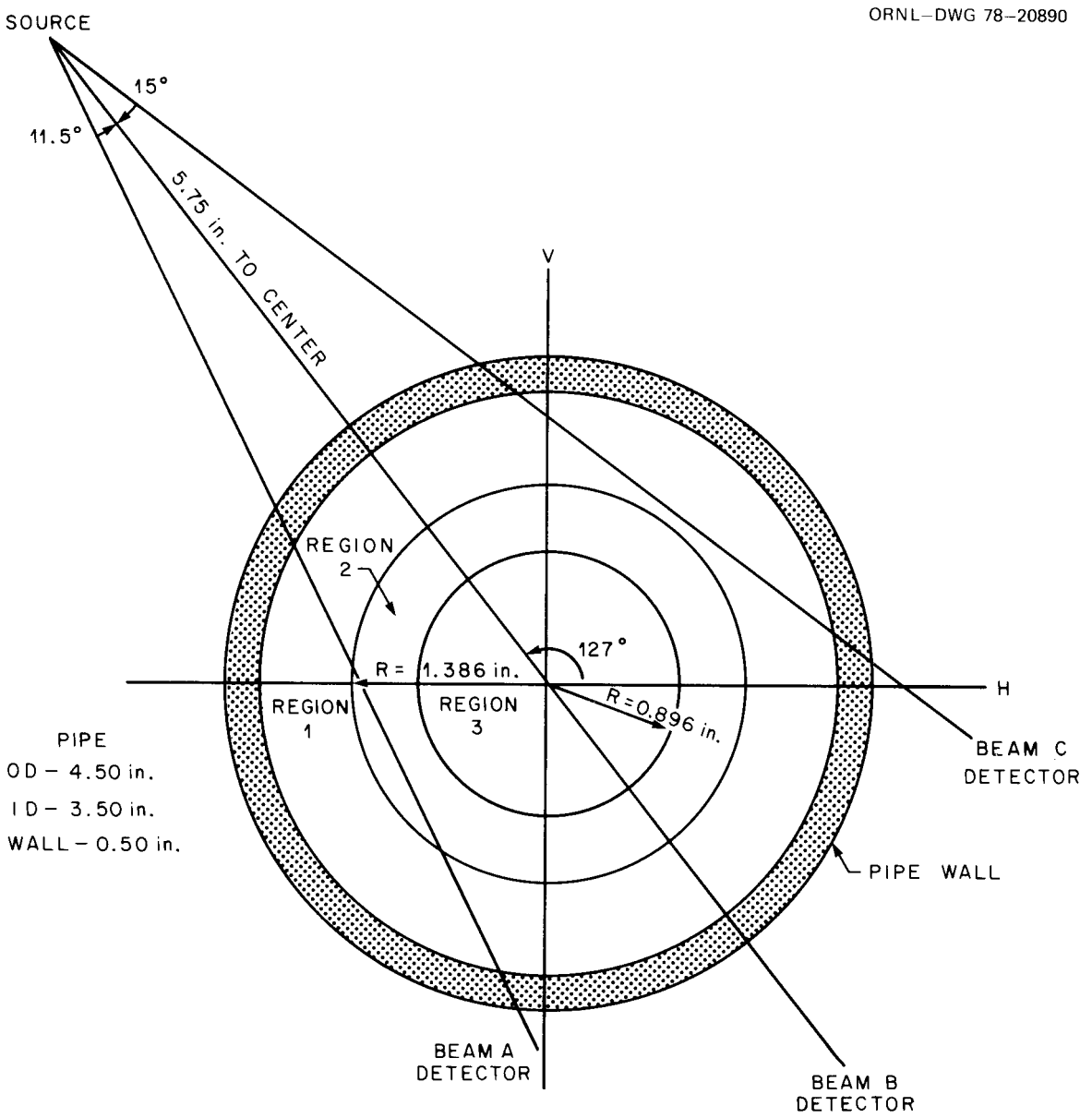

Fig. 3.1. Cross-sectional view of paths of densitometer beams and three regions used for calculation of composite density.

the beams is assumed to be expressed as follows:

$$\rho_a = \frac{1}{\ell_a} [\ell_{a1}\rho_1 + \ell_{a2}\rho_2] , \tag{8}$$

$$\rho_b = \frac{1}{\ell_b} [\ell_{b1}\rho_1 + \ell_{b2}\rho_2 + \ell_{b3}\rho_3] , \tag{9}$$

and

$$\rho_c = \rho_1 \ , \tag{10}$$

where ℓ_a and ℓ_b are the total lengths within the pipe of beams A and B and ℓ_{ij} is the length of beam i which lies within region j.

Substituting Eq. (9) into Eq. (7) and solving for ρ_2,

$$\rho_2 = \frac{1}{\ell_{a2}} [\rho_a \ell_a - \ell_{a1}\rho_c] \ . \tag{11}$$

The density of region 3, the center region, may be evaluated using Eq. (9), where ρ_2 may be evaluated using Eq. (11).

$$\rho_3 = \frac{1}{\ell_{b3}} [\rho_b \ell_b - \ell_{b1}\rho_c - \ell_b \rho_2] \ . \tag{12}$$

The composite density in the pipe $\overline{\rho}$ is then given by

$$\overline{\rho} = \frac{1}{A_{tot}} [A_1\rho_1 + A_2\rho_2 + A_3\rho_3] \ , \tag{13}$$

where A_1, A_2, A_3, and A_{tot} are the cross-sectional areas of regions 1, 2, and 3 and the total pipe area, respectively.

4. EXPERIMENTS PERFORMED

During the current quarter, experiments were conducted in the air-water loop using advanced spool piece I with the drag targets described in the previous report.[8] For these runs, the spool piece was oriented horizontally, with the drag flowmeter adapters on top of the pipe and the pressure taps on the bottom of the pipe. Each of the drag targets was tested in the spool piece with no flow-dispersing screens. In addition, runs were made to investigate the effect of flow-dispersing screens on the performance of the instruments. Both 4-20 screens and 2-20 screens were used. (A 4-20 screen has four stacked layers of 20 mesh/in. screen; a 2-20 screen has two stacked layers of 20-mesh/in. screens.)

Preliminary analysis of data from most of the experiments has been performed. It is not yet possible to make judgments regarding the relative merits of the drag target design or to evaluate the overall spool piece design. Work is continuing in these areas.

5. RESULTS

5.1 Individual Instrument Response

Before discussing mass flux calculations performed using data from the spool piece instruments, some instrument signal outputs vs time will be shown. Figures 5.1—5.3 show instrument outputs taken at 7.5 liters/sec (16 scfm) air flow rate with three water flow rates. The data are from run 7, in which a three-bladed drag target and no flow-dispersing screens were used in the spool piece. The flow regimes indicated are a slow slug flow at 1.9 liters/sec (30 gpm) (Fig. 5.1), a rapid slug flow at 19 liters/sec (300 gpm) (Fig. 5.2), and a nearly dispersed air-water mixture at 28 liters/sec (450 gpm) (Fig. 5.3). (See also Fig. 2.2, 16 scfm.) Looking from the top to the bottom of the figures, the signal traces are from the instruments that would be encountered when proceeding through the spool piece in the normal direction of flow (Fig. 1.1). All three densitometer beams are at the same axial location.

Figure 5.1, slow slug flow, represents 20 sec of data. Comparing the response of the instruments to passage of a slug is interesting. The drag flowmeters, gamma densitometer beams, and pressure difference cell all respond fairly quickly to arrival of the disturbance, while the turbine meter responds slowly and poorly simulates the duration of the slug detected by the other instruments. Between slugs, the turbine meter does not respond. This problem is related to the electronics used to process the turbine meter signal. The densitometer signals clearly indicate that slugs filled the pipe completely for brief instants on four occasions during the scan period (beam C) and that, between slugs, the top of the pipe was completely empty. From a comparison of the front and rear drag flowmeter signals, it is apparent that the slugs were moving rapidly, taking only a few tenths of a second to traverse the spool.

At 19 liters/sec (300 gpm) (Fig. 5.2), the slug frequency is much higher, $\sim$5 Hz. Note that only 5 sec of data are plotted. Again, the drag disk and densitometer time responses are adequate, but the turbine meter response is not. Note that the signal character from the two drag

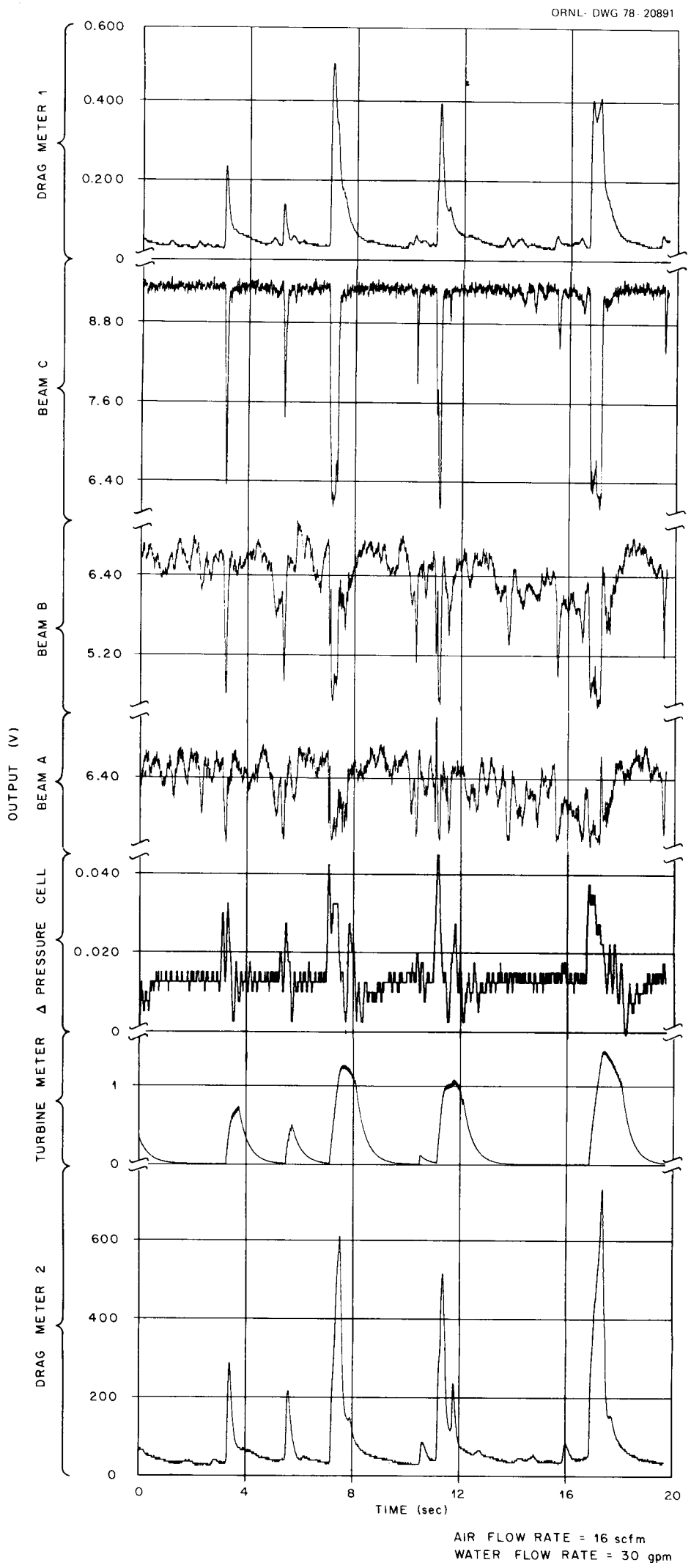

Fig. 5.1. Voltage output vs time from spool piece instrumentation, run 7, 7.5 liters/sec (16 scfm) air, 1.9 liters/sec (30 gpm) water.

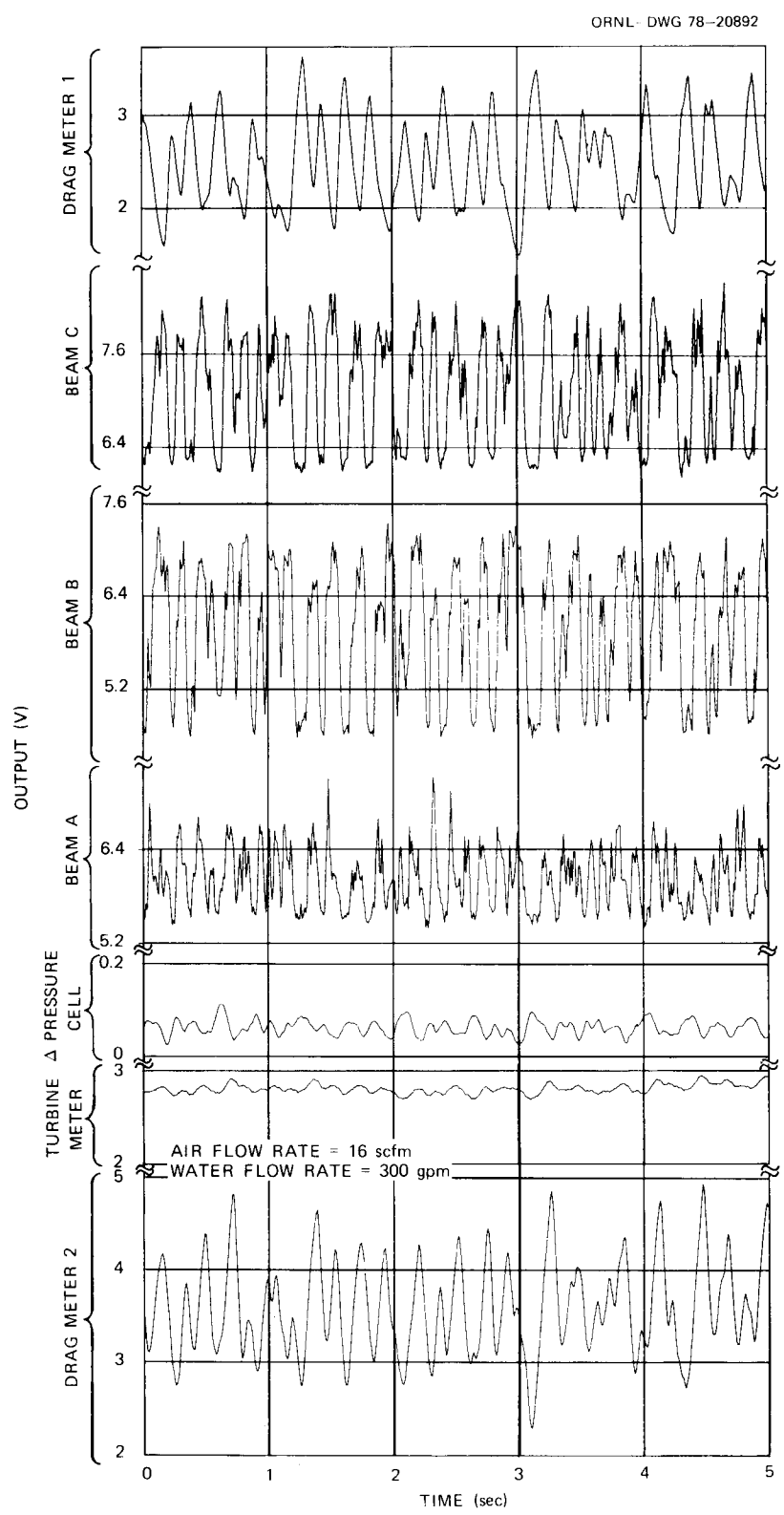

Fig. 5.2. Voltage output vs time from spool piece instrumentation, run 7, 7.5 liters/sec (16 scfm) air, 19 liters/sec (300 gpm) water.

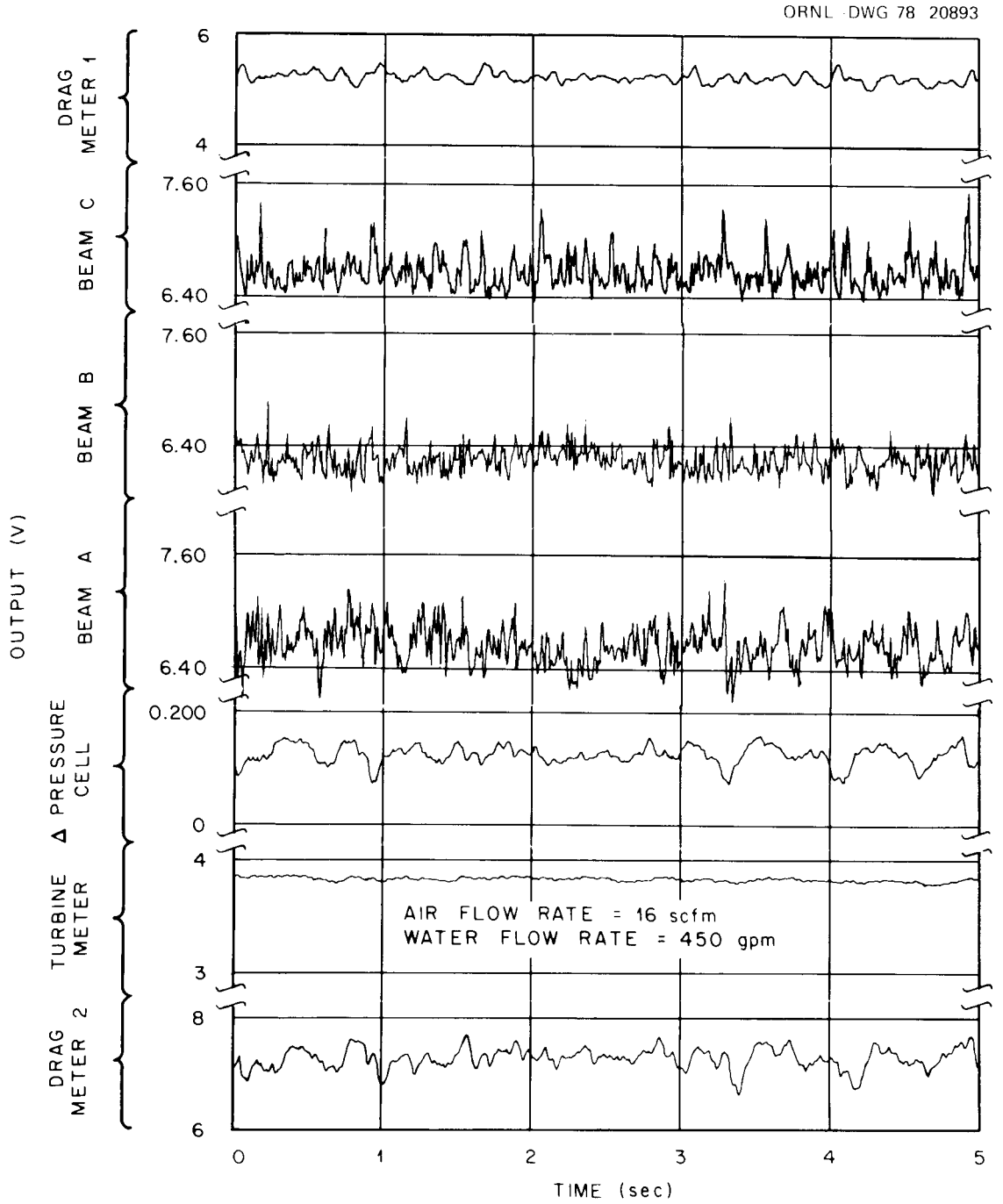

Fig. 5.3. Voltage output vs time from spool piece instrumentation, run 7, 7.5 liters/sec (16 scfm) air, 28 liters/sec (450 gpm) water.

flowmeters is similar, even though the fluid passing the downstream meter has just passed through the turbine meter. A visual check suggests that the passage time between the two drag meters is ∿0.15 sec. In such flow regimes, significant errors will occur if instantaneous instrument signals from stations separated by more than 3.1 m (1 ft) are used in two-phase models.

With a further increase in flow to 28 liters/sec (450 gpm) (Fig. 5.3), a radical change in flow regime occurs. As the slugging subsides, a churning or frothy dispersed flow occurs. Errors due to physical separation of instruments are minimal here because signal-variation/signal-mean ratios are now quite small. The turbine meter signal output behaves as though the flow is single phase. Variations in the two drag flowmeter signals are still alike, but the spool piece transit time is now very short. The three densitometer beams are very much alike in character, with little oscillation. This suggests an approach to homogeneous conditions.

A complete set of data from one of the experiments (run 7) will be shown and briefly described here. For the graphs shown, all data with a given symbol type were taken at the same air flow rate (see legends inside figures). Quality is defined here as mass flow rate of air divided by the total metered input mass flow rate. The highest quality plotted at a given air flow rate was for a water flow rate of only 0.6 liter/sec (10 gpm). Increasingly higher water flow rates result in data points to the left of the 0.6-liter/sec (10-gpm) point. In terms of flow regime, the points with highest quality were in stratified flow (Fig. 2.2). As water flow was increased, a slug flow regime developed. This persisted until the flow became dispersed at a flow rate of ∿25 liters/sec (∿400 gpm). At the highest air flow rates [121 and 242 liters/sec (256 and 512 scfm)], considerable entrainment of water in the gaseous layer occurred, with annular films often covering the sides and top of the pipe.

The average densities computed (as described previously) are graphed in Fig. 5.4. As a reference, the density calculated from the metered air and water inputs assuming a slip (vapor velocity/liquid velocity) equal

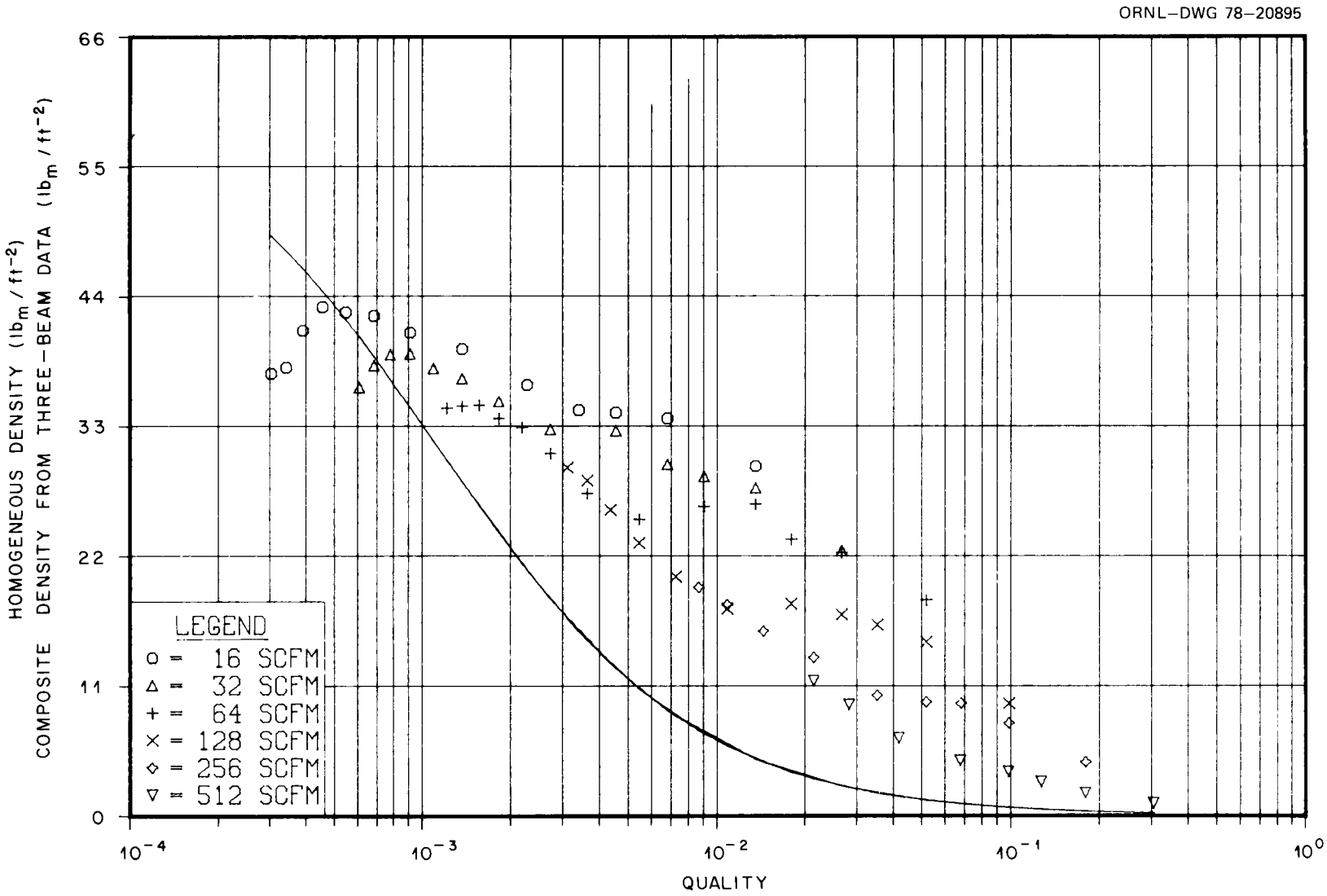

Fig. 5.4. Average composite density vs quality, run 7, and location of homogeneous density (solid line) for comparison.

to unity is also plotted. Because of holdup of the liquid, the measured density was greater than the homogeneous density for most of the flow rates. The void fractions represented by the data appear in Fig. 5.5. They may be calculated from

$$\alpha = \frac{\rho_f - \overline{\rho}}{\rho_f - \rho_g} , \tag{14}$$

where $\overline{\rho}$ is the density plotted in Fig. 5.4. The densitometer was located ∿15 cm (∿6 in.) downstream of a full-flow drag target (a three-bladed design — number five in Table 1 of Ref. 8), but no flow dispersers were present for this run. Some perturbation in the flow regime which existed upstream of the test section was probably caused by the presence of the drag target. Comparison of densities taken from runs with the 1.3-cm (0.5-in.) target (Fig. 5.6) suggests that the effect was most serious at very low qualities where the measured density was less than the homogeneous density.

The average turbine meter velocities V_t obtained using Eq. (1) are shown in Fig. 5.7 as a function of quality. In general, successively higher water inputs at a given air input (a common graph symbol type) result in increased average turbine meter output. At 242 liters/sec (512 scfm), however, increasing water input served to slow the turbine. Several points taken had essentially zero output from the turbine meter electronics. Other points, some of which are shown in Fig. 5.7, had intermittent output as fast-moving slugs of water sometimes caused the pulse rate received to briefly exceed the minimum frequency threshold.

The three-bladed target was oriented for test 7 as shown in Fig. 5.8. The fluid momentum fluxes indicated by the upstream drag disk in the spool piece (Fig. 5.9) ranged from 150 to 27,000 kg/m-sec^2 (100 to 18,000 lb_m/ft-sec^2). There is a 15-mV positive zero shift in this drag disk data which was not allowed for in Fig. 5.6 or in subsequent analysis using drag flowmeter data shown in this report. For the three-bladed target, the zero shift represents a momentum flux of 64 kg/m-sec^2 (43 lb_m/ft-sec^2).

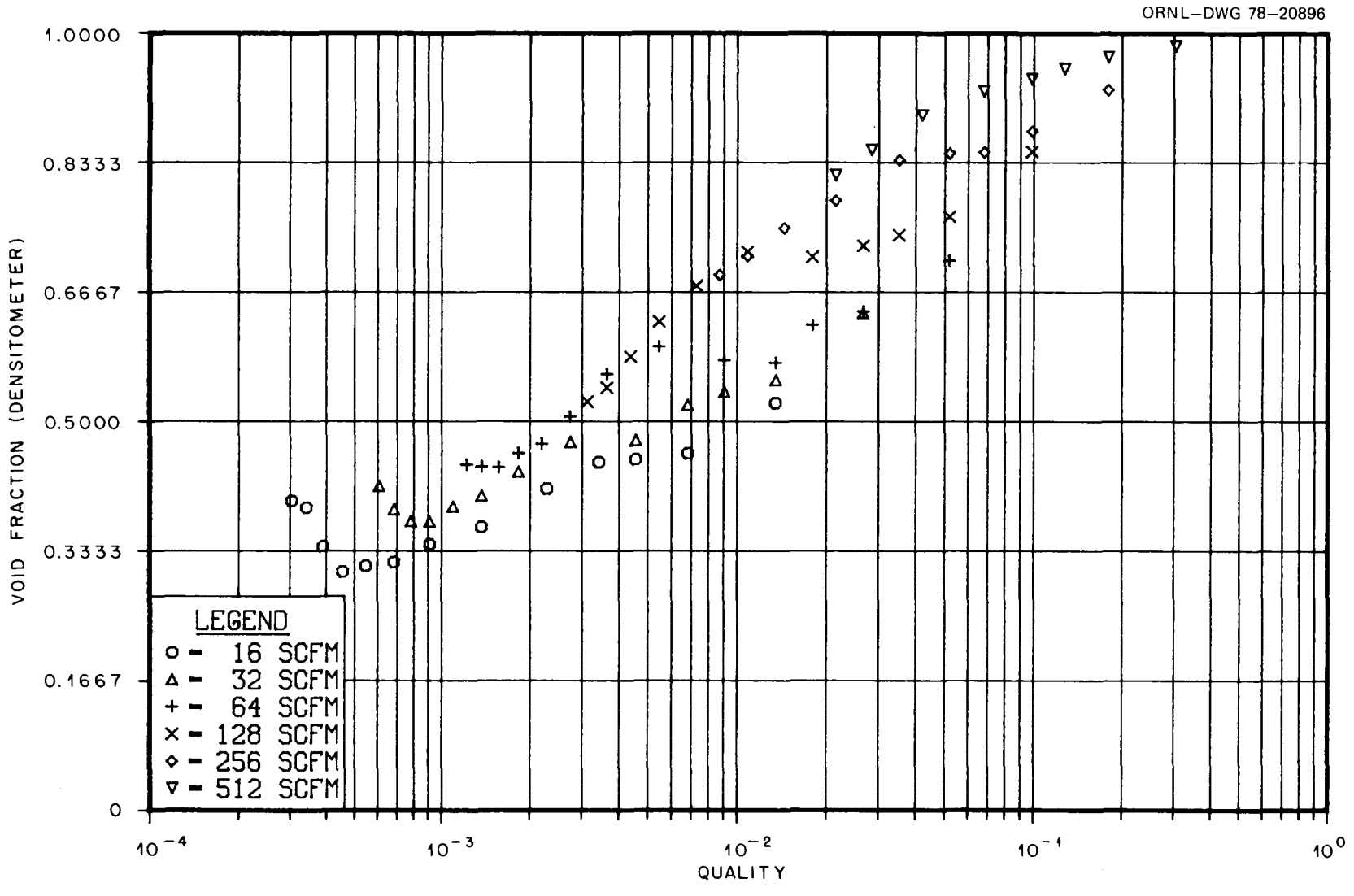

Fig. 5.5. Average void fraction vs quality, run 7.

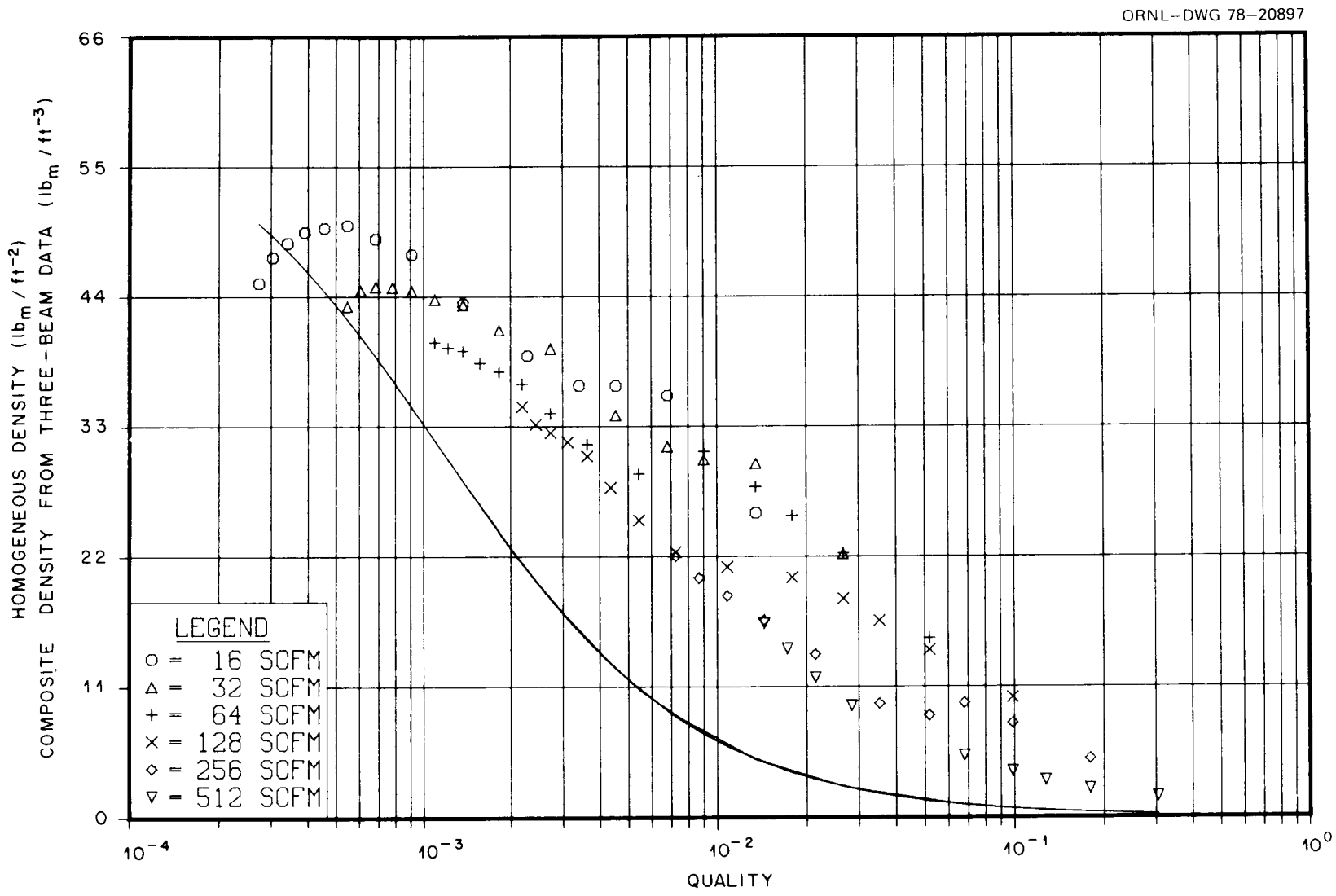

Fig. 5.6. Average composite density vs quality, runs 1 and 2, and location of homogeneous density (solid line) for comparison.

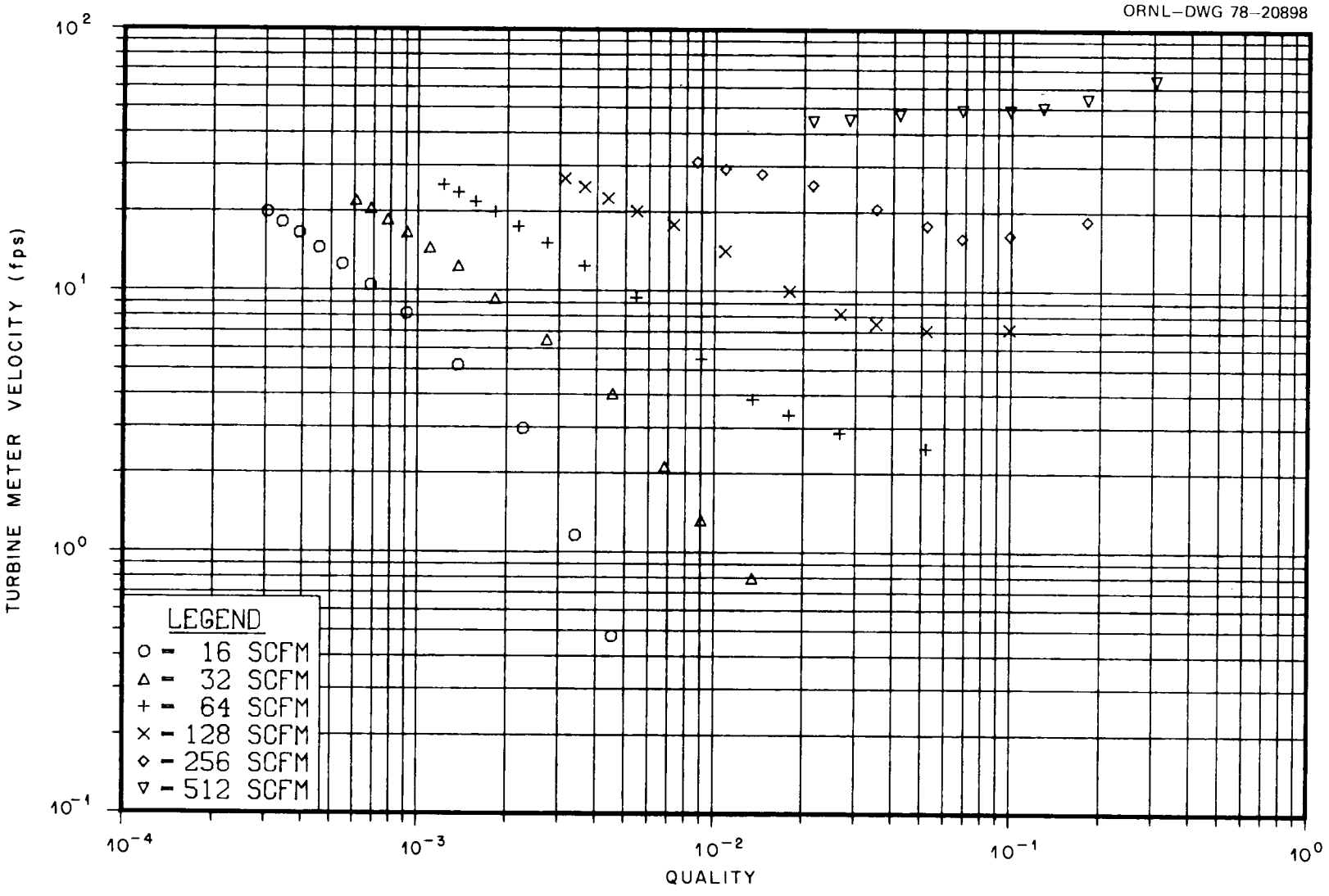

Fig. 5.7. Average turbine velocity V_t vs quality, run 7.

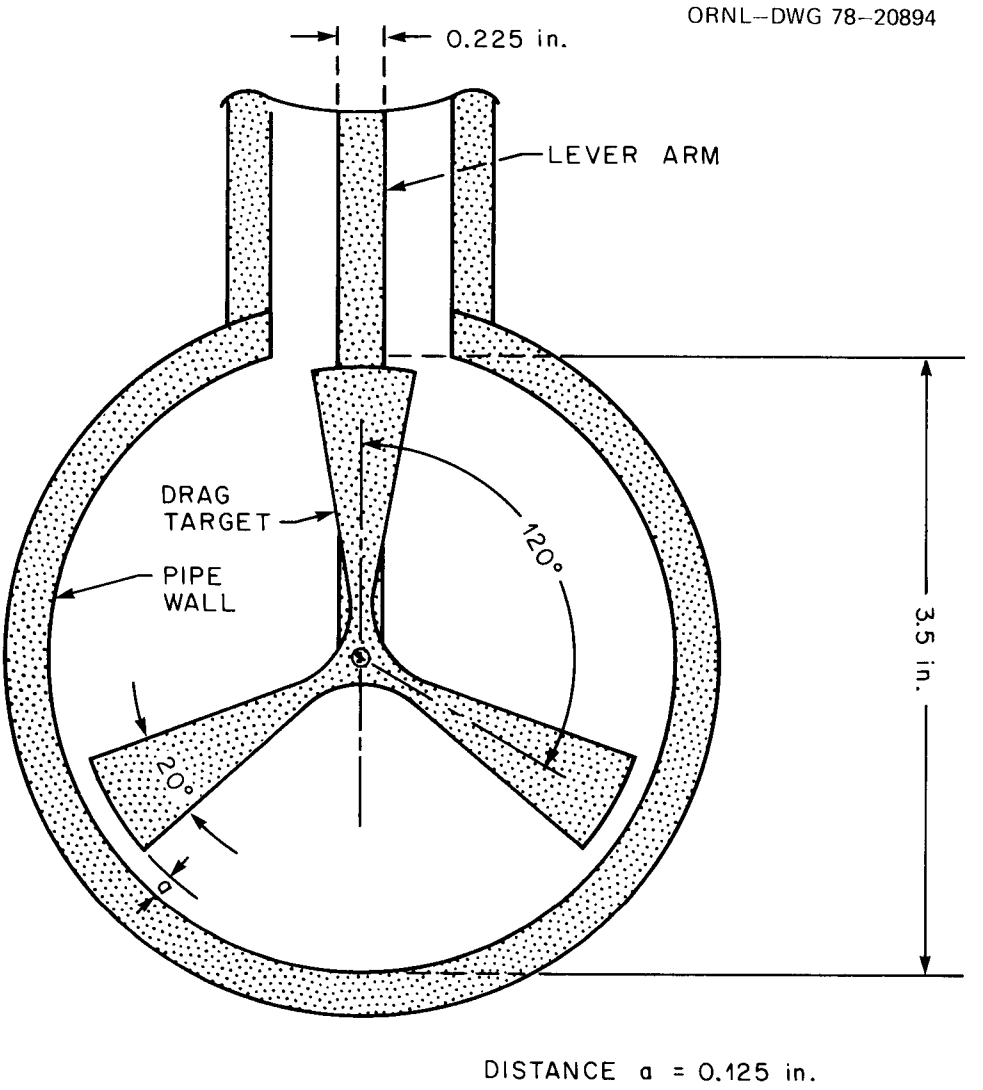

Fig. 5.8. Appearance of three-bladed drag target in pipe for run 7. View is looking downstream.

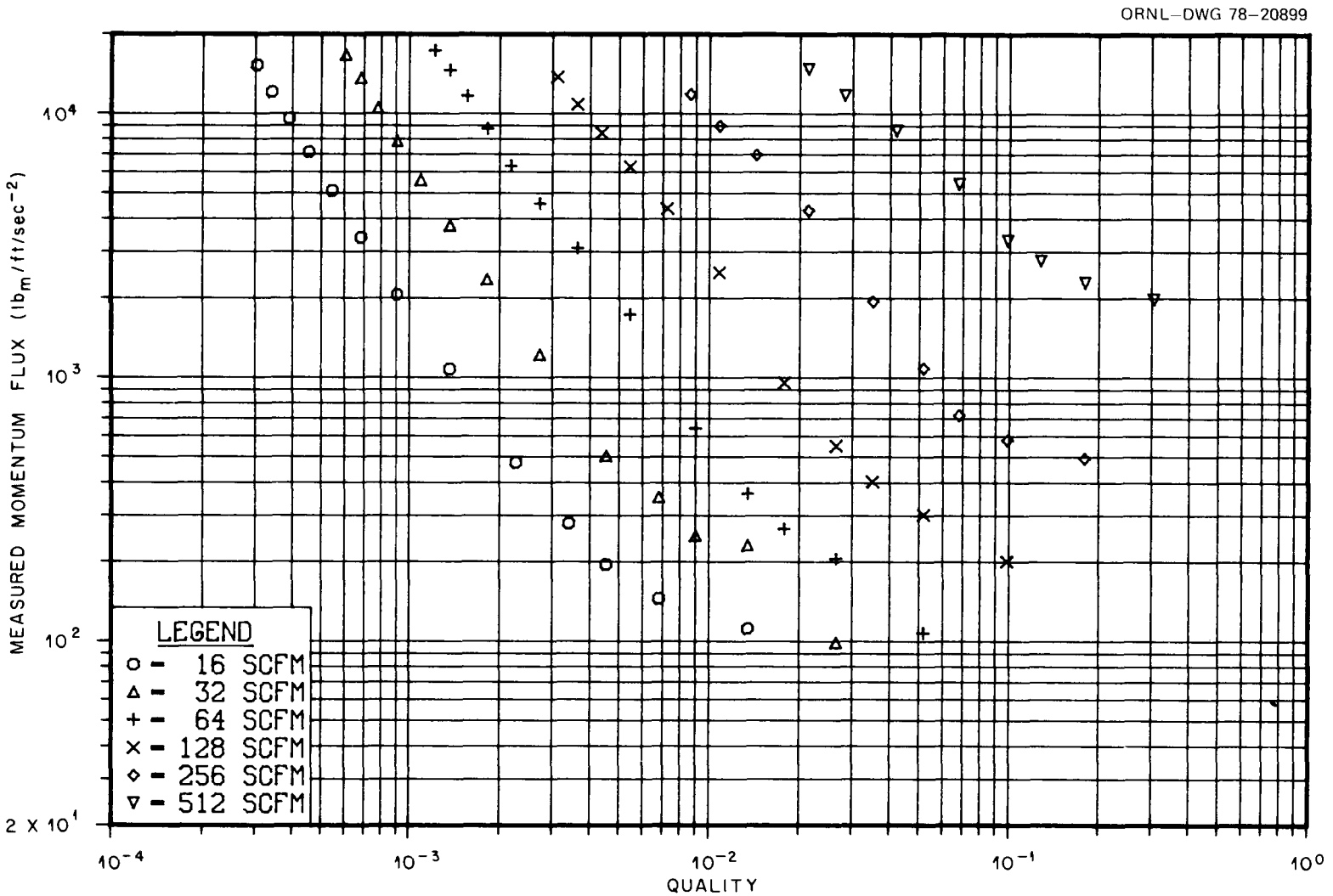

Fig. 5.9. Average momentum flux I_d vs quality, run 7. All data are shifted 43 $lb_m/ft/sec^2$ upward due to 15 mV zero shift.

5.2 Mass Flux Calculations

Preliminary results of mass flux calculations made with data from advanced spool piece I appear in Figs. 5.10 through 5.12. The abscissa of the plots are like those in Figs. 5.4, 5.7, and 5.9. The ordinates are of the form $G_{model}/G_{metered}$, where G_{model} is one of the three homogeneous models and $G_{metered}$ is the "true" mass flux based on the air and water input rates to the loop. For each point shown, the procedure used to calculate the modeled mass flux involved the manipulation of mean instrument readings, averaged over a 20-sec scan. For the graphs shown here, model calculations were not made instantaneously or over small time intervals, as might be done during analysis of blowdown data. Efforts to evaluate the effects of this are under way.

If homogeneous flow in the spool piece is assumed, any two of the three primary spool piece instruments may be used to calculate the mass flux. Perhaps the most commonly used method is multiplication of the volumetric flow indicated by the turbine meter by the composite (average) density calculated from densitometer data. The appropriate ratio is plotted in Fig. 5.10. The turbine meter response for low water flow rates at low air flow rates [7.5 and 15 liters/sec (16 and 32 scfm)] is often intermittent (see Fig. 5.1). For this reason, modeling of such flow rates using the turbine meter with the Flow Technology electronics results in serious errors. The points encircled by a dashed line in Figs. 5.10 and 5.12 suffered from that problem. At qualities of <1%, the model does reasonably well. This may be explained as follows. For low qualities, the two-phase mass flux may be approximated as follows:

$$G \cong G_f = \frac{\rho_f V_f A_f}{A_t} = (1 - \alpha)\rho_f V_f \ . \tag{15}$$

Now compare the average turbine meter response to the average liquid velocity V_f. The latter may be determined from a mass balance on the liquid phase. We have

$$w_{ts} = w_{input} \ , \tag{16}$$

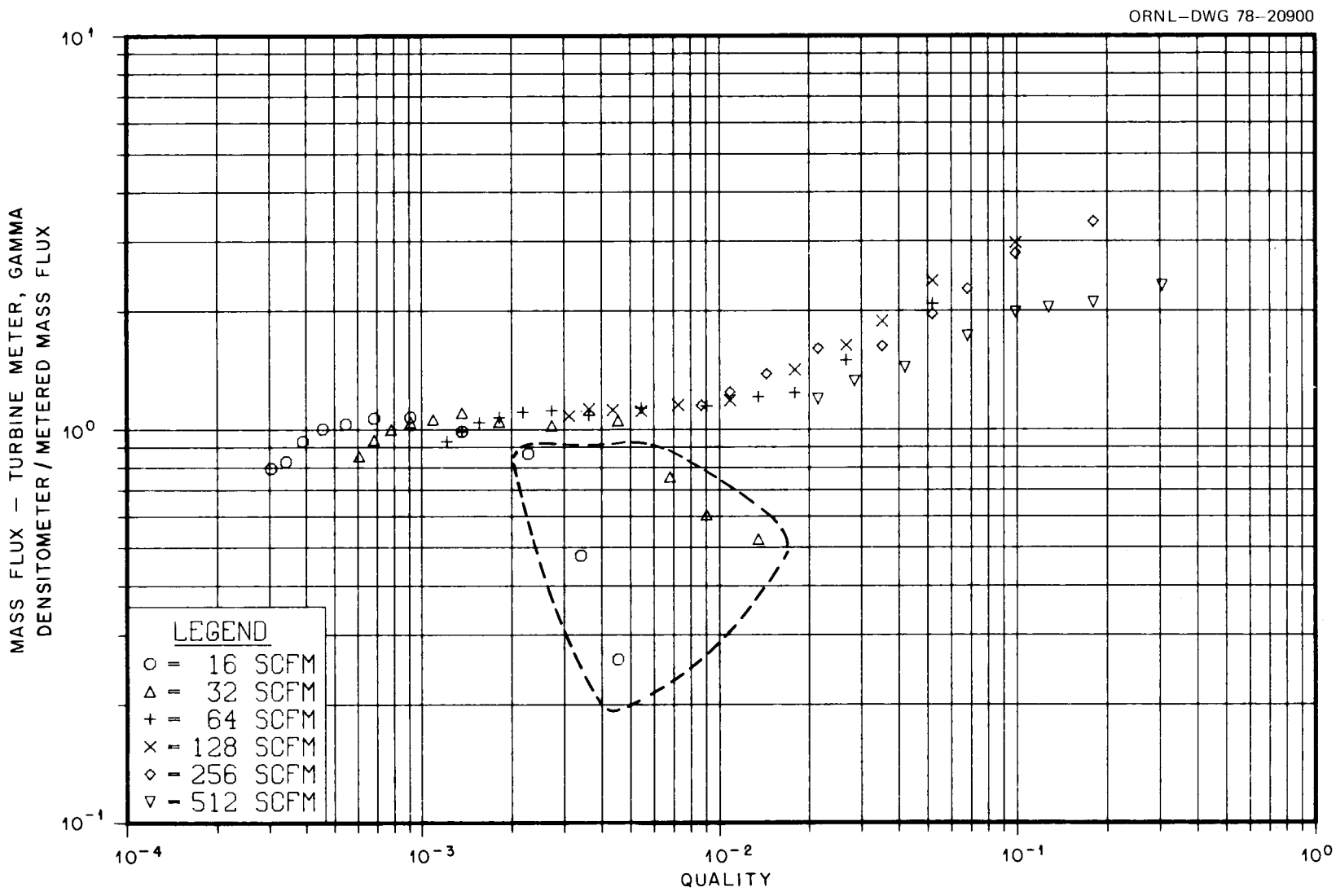

Fig. 5.10. Ratio of mass flux calculated using $G = \overline{\rho} V_t$ to G_{actual} vs quality, run 7. For points inside dashed line, turbine meter was intermittent.

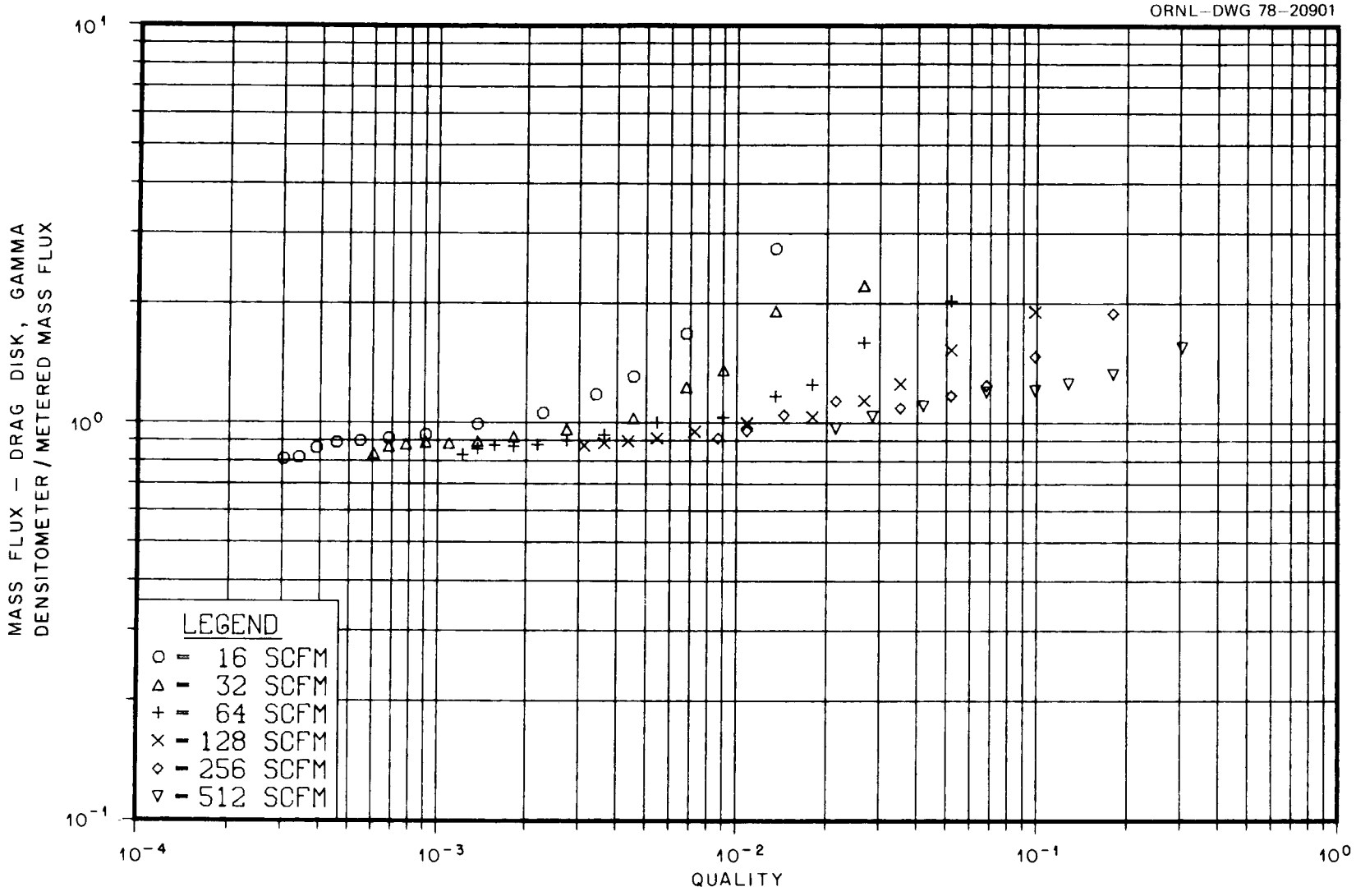

Fig. 5.11. Ratio of mass flux calculated using $G = (\overline{\rho} I_d)^{1/2}$ to G_{actual} vs quality, run 7. Drag flowmeter readings I_d have 15-mV (43-lb_m/ft/sec^2) positive zero shift which was not accounted for in this model.

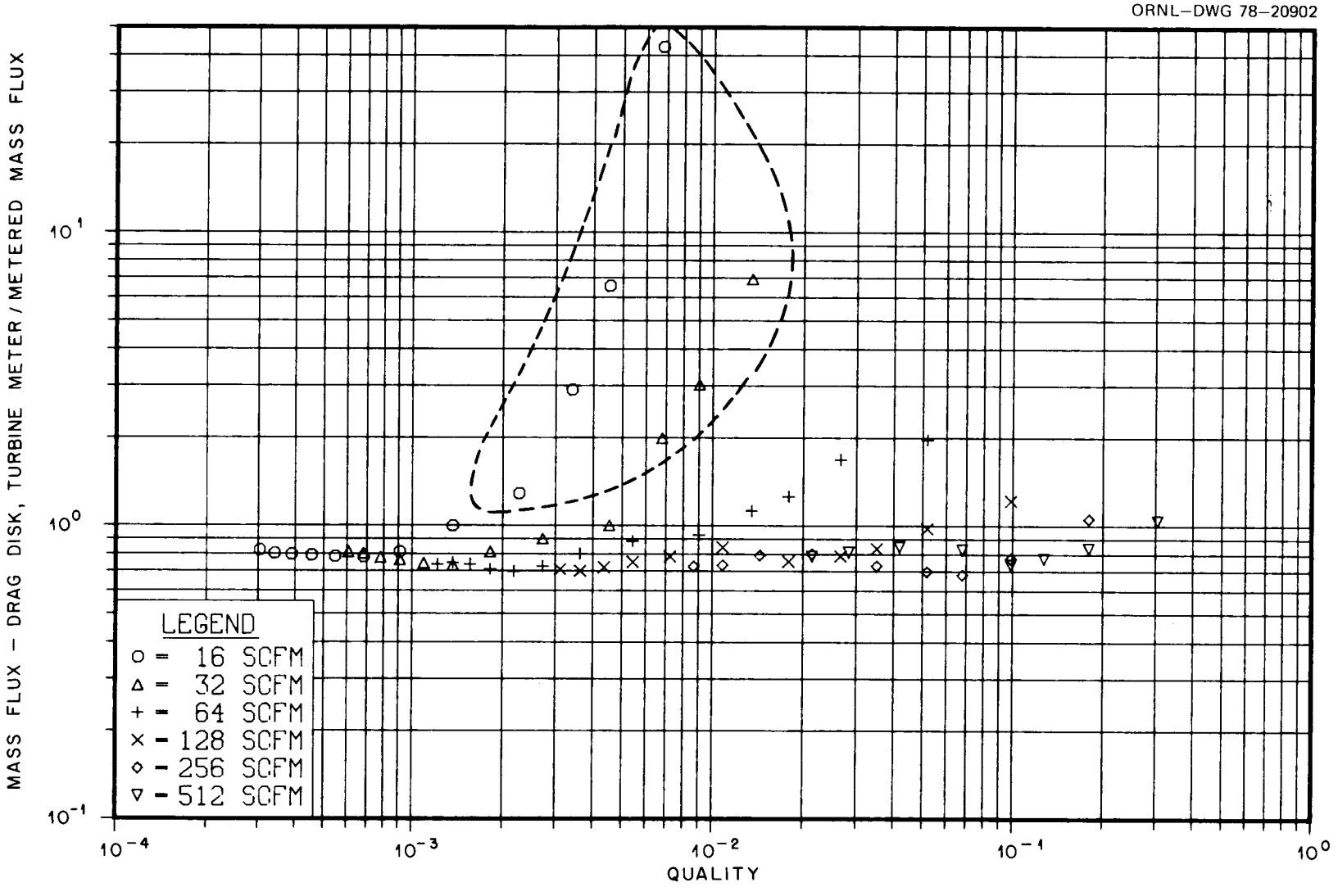

Fig. 5.12. Ratio of mass flux calculated using $G = I_d/V_t$ to G_{actual} vs quality, run 7. Drag flowmeter readings I_d have 15-mV (43-lb_m/ft/sec^2) positive zero shift which was not accounted for in this model.

where w_{ts} and w_{input} are the mass flow rates of liquid in the test section and at the metering station, respectively. Also

$$\rho_f V_f A_f = \rho_f Q_f \ . \tag{17}$$

Canceling liquid densities, we obtain

$$V_f = \frac{Q_f}{(1 - \alpha)A_t} \ . \tag{18}$$

This quantity is plotted for run 7 in Fig. 5.13. Comparing data from Figs. 5.7 and 5.13, for qualities <1%, it is clear that $V_f \cong V_t$. This is true except at very low flow rates when the turbine meter output signal is intermittent. Using Eq. (14), one sees that, for low qualities,

$$\overline{\rho} \cong (1 - \alpha)\rho_f \ . \tag{19}$$

Therefore, substituting Eqs. (19) and (18) into Eq. (15), the actual mass flux is given by the product of turbine meter and densitometer signals. The rolloff of data at the lowest qualities is due to the unreasonably low densities calculated for those flow rates (see Fig. 5.4). For qualities >1%, two things happen — the turbine meter signal begins to appreciably exceed the liquid velocity, and the ratio of gas to liquid velocities becomes progressively higher. A model that takes these factors into account is required for accurate prediction of mass flow at higher qualities.

A second, often-used combination of instruments is given by the following equation:

$$G = (\overline{\rho} I_d)^{1/2} \ . \tag{20}$$

The results obtained from applying Eq. (20) to run 7 (using the three-bladed drag target data) appear in Fig. 5.11. For a given air flow rate, the data for low water flow are well above unity, but these data decrease and become fairly constant at ∿90% of the correct value. The overestimate of the mass flux at low air-water flow rates is partially due to the 15-mV

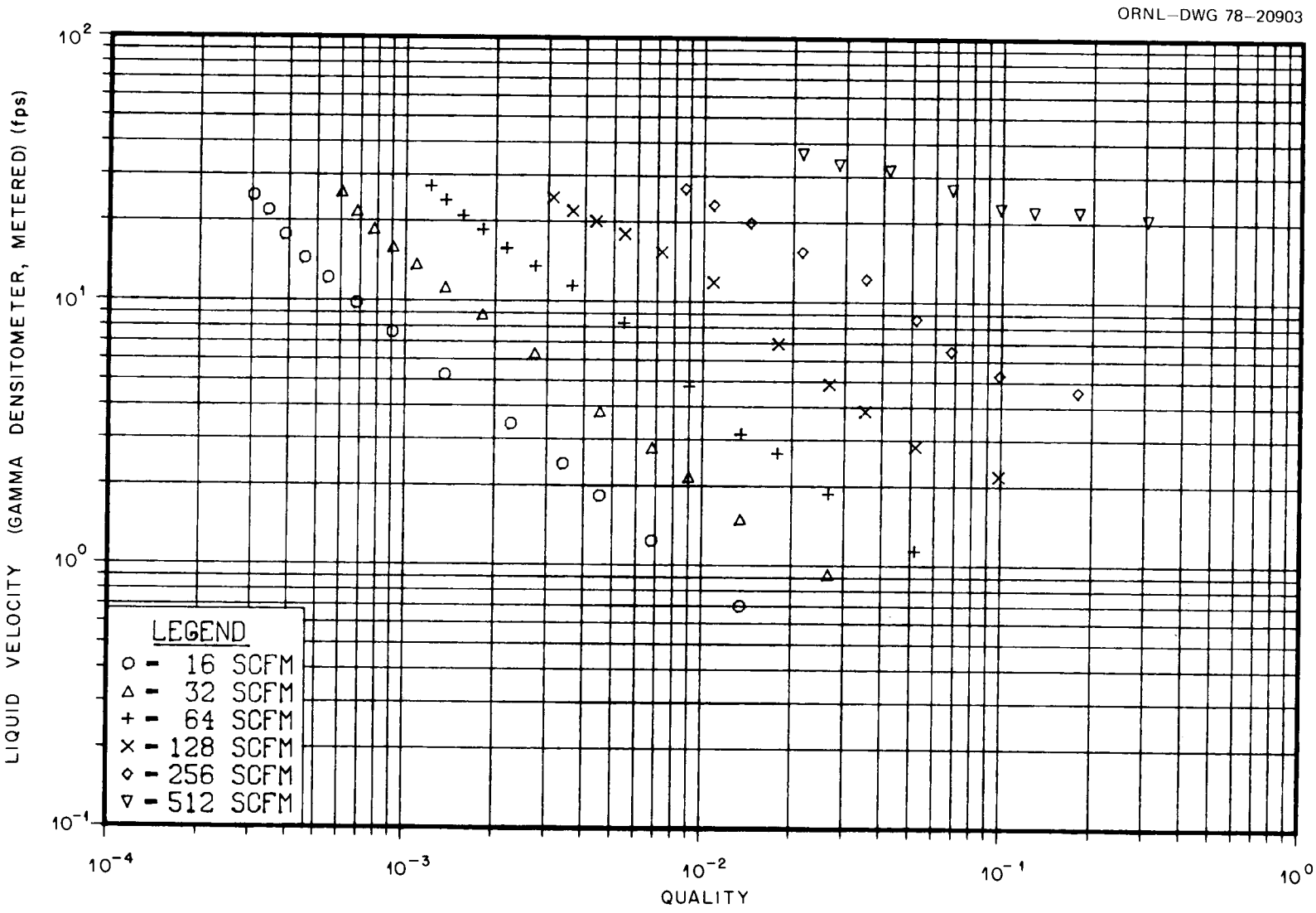

Fig. 5.13. Mean liquid velocity V_f in spool piece in quality, run 7.

zero shift mentioned previously. The other error is perhaps due to the nature of the flow (slow slugging) at these rates and to the method used to average the data. These effects are being studied.

Data from run 7 were also processed using a third method — dividing the drag flowmeter reading by the turbine meter reading (Fig. 5.12). At very low flow rates, the intermittency of the turbine meter output results in an overestimate of the actual mass flux by the model (encircled points). For the other data, the performance of the model is relatively consistent. This model has the interesting characteristic of applying equally well for the homogeneous assumption or a two-velocity assumption, when the turbine meter response is postulated to be like that of the Rouhani-Estrada model.[10] That model suggests that

$$V_t = \frac{(1-\alpha)\rho_f V_f^2 + \alpha\rho_g V_g^2}{(1-\alpha)\rho_f V_f + \alpha\rho_g V_g} . \tag{21}$$

Also, the two-velocity assumption for drag target behavior used by both Aya[11] and Rouhani is

$$I_d = C_{df}(1-\alpha)\rho_f V_f^2 + C_{dg}\alpha\rho_g V_g^2 , \tag{22}$$

where C_{df} and C_{dg} are drag coefficients for liquid and vapor phases, respectively. Further, in the two-velocity model, the mass flux is given by

$$G = (1-\alpha)\rho_f V_f + \alpha\rho_g V_g . \tag{23}$$

Assuming $C_{df} = C_{dg} = 1$ and substituting Eqs. (22) and (23) into Eq. (21),

$$V_t = I_d/G , \tag{24}$$

or

$$G = I_d/V_t . \tag{25}$$

It appears from Fig. 5.12 that the model is consistent and would predict a nearly correct mass flow if a constant two-phase drag coefficient of

some 30% lower for two-phase flow were assumed [a lower drag coefficient means a higher value of the constant a in Eq. (2)].

6. SUMMARY AND CONCLUSIONS

Testing of advanced spool piece I in a horizontal orientation in the ORNL air-water loop is in progress. Two-phase experiments with a number of drag targets and with and without flow-dispersing screens have been performed. Analysis of the data is in progress.

Preliminary conclusions included the following:

1. At low air flow rates with low water flow rates, the turbine system response using the Flow Technology electronics results in poorly predicted mass fluxes.

2. At moderate-to-high air and water flow rates and qualities <1% (void fractions less than ∿50%), use of the models $G = V_t\bar{\rho}$ and $G = (\bar{\rho}I_d)^{1/2}$ leads to good estimates of mass flux in the air-water system.

3. Use of the models under item 2 above results in gross overprediction of the mass flux for qualities >1% in the air-water system.

4. Using data from a three-bladed, full-flow drag target, preliminary analysis of the spool piece data using a two-velocity drag target assumption and a Rouhani turbine meter assumption yields consistent results over a wide range of quality in the air-water system. (The model is calculated as $G = I_D/V_t$.) If a constant two-phase drag coefficient of some 30% lower than the single-phase drag coefficient is assumed, good agreement with the measured values is obtained.

REFERENCES

1. *Project Description ORNL-PWR Blowdown Heat Transfer Separate Effects Program — Thermal-Hydraulic Test Facility (THTF)*, ORNL/NUREG/TM-2 (February 1976).

2. E. M. Feldman and D. J. Olson, *Semiscale MOD-1 Program and System Description for the Blowdown Heat Transfer Tests (Test Series 2)*, Idaho National Engineering Laboratory Report No. ANCR-1230 (August 1975).

3. J. D. Sheppard, P. H. Hayes, and M. C. Wynn, "An Experimental Study of Flow Monitoring Instruments in Air-Water Two-Phase Downflow," presented at OECD/NEA Symposium on Transient Two-Phase Flow, Toronto, Canada, August 1976.

4. J. D. Sheppard et al., *Quarterly Progress Report on the Advanced Two-Phase Instrumentation Program for January—March 1977*, ORNL/NUREG/TM-119 (July 1977).

5. *Quarterly Progress Report on Reactor Safety Programs Sponsored by the Division of Reactor Safety Research for July—September 1974, Vol. I, Light-Water Reactor Safety*, ORNL/TM-4729, Vol. I (December 1974), pp. 42—51.

6. J. D. Mandhane et al., "A Flow Pattern Map for Gas-Liquid Flow in Horizontal Pipes," *Int. J. Multiphase Flow*, Vol. I, pp. 537—53, 1974.

7. R. M. Flanders, "Description and Set-Up Procedure for the Two-Phase Engineering Units Code," Oak Ridge National Laboratory unpublished internal report.

8. K. G. Turnage et al., *Quarterly Progress Report on the Advanced Two-Phase Instrumentation Program for January—March 1978*, ORNL/NUREG/TM-250.

9. Y. Y. Hsu and R. W. Graham, *Transport Processes in Boiling and Two-Phase Systems*, Hemisphere Publishing Corporation, Washington, D.C., 1976, pp. 381—85.

10. MPR Associates, Inc., *Interpreting Two-Phase Flow Measurements*, MPR-511 (May 1976).

11. Izuo Aya, *A Model to Calculate Mass Flow Rate and Other Quantities of Two-Phase Flow in a Pipe with a Densitometer, a Drag Disk, and a Turbine Meter*, ORNL/TM-4759 (November 1975).

NUREG/CR-0501
ORNL/NUREG/TM-279
Dist. Category R2

Internal Distribution

1. R. S. Booth
2. S. B. Cliff
3. S. K. Combs
4. W. B. Cottrell
5. W. G. Craddick
6. C. E. Davis
7. I. T. Dudley
8. B. G. Eads
9. R. C. Hagar
10. J. E. Hardy
11. M. Herskovitz
12. H. W. Hoffman
13. W. H. Leavell
14. R. N. McGill
15. F. R. Mynatt
16. H. Postma
17. M. J. Roberts
18-19. M. R. Sheldon
20. D. G. Thomas
21. H. E. Trammell
22. D. B. Trauger
23. K. G. Turnage
24. M. D. White
25. J. D. White
26. ORNL Patent Office
27-28. Central Research Library
29. Document Reference Section
30-32. Laboratory Records Department
33. Laboratory Records (RC)

External Distribution

34-41. Director, Division of Reactor Safety Research, Nuclear Regulatory Commission, Washington, D.C. 20555
42. Director, Reactor Division, DOE, ORO
43. Office of Assistant Manager, Energy Research and Development, DOE, ORO
44-48. Director, Reactor Safety Research Coordination Office, DOE, Washington, D.C. 20555
49-363. Given distribution as shown in category R2 (TIC-2, NTIS-25)

☆U.S. GOVERNMENT PRINTING OFFICE: 1979-748-189/383